# Supplementary Information

# Populating surface-trapped electrons towards SERS enhancement of $W_{18}O_{49}$ nanowires

## Experiment methods

**Synthesis of sea-urchin-like $W_{18}O_{49}$ nanostructures.** $W_{18}O_{49}$ nanowires in sea-urchin-like morphology were prepared through hydrothermal approach [1]. Briefly, $WCl_6$ (0.099 g) was dissolved in 30 mL absolute ethanol and subsequently transferred to a Teflon-lined stainless steel autoclave, which was then sealed and heated at 180 °C for 12 h. After finishing the reaction, the blue sediments were collected by centrifugation and rinsed thoroughly with absolute ethanol before drying naturally at room temperature.

**$W_{18}O_{49}$ nanostructures loaded with Ag/Pt/Au/Pd nanoparticles.** Ag nanoparticles were deposited on the as-prepared $W_{18}O_{49}$ at room temperature by means of photocatalytic reaction [2]. 30 mg $W_{18}O_{49}$ was dispersed into 30 mL distilled water. 0.084 mL $AgNO_3$ aqueous solution (0.1 M) was added into the $W_{18}O_{49}$ suspension after stirring for 2 h. Then the suspension was illuminated by xenon lamp for 2 h with continuous stirring. Similarly, Pt nanoparticles were loaded on $W_{18}O_{49}$ using the same way except that $AgNO_3$ aqueous solution was replaced by $H_2PtCl_6$ aqueous solution. While for Au and Pd nanoparticles loading, the precursor used was $HAuCl_4$ and $PdCl_2$, respectively.

**Raman measurement.** To study the Raman enhancement effect by the tungsten oxide materials, Rhodamine 6G (R6G) dissolved in deionized water was employed as the probe molecule, with the tested concentration of $10^{-5}$ M. After dropping an aliquot of the respective solutions on the substrate and drying for at least 5 h, Raman spectra were subsequently collected on a high-resolution confocal Raman spectrometer (LabRAM HR-800) using the same instrumental settings for ready comparisons. The excitation wavelength was 532.8 nm and a 50 × L objective was used to focus the

laser beam. The spectra were acquired for 30 s with 3 accumulations and the laser power was maintained at 0.3 mW with an average spot size of 1 μm in diameter in all acquisitions. For each sample, Raman spectra from at least ten different areas were collected, and the signal intensity was averaged for final analysis, from which values of enhancement factor (EF) values were calculated with error bars.

**Calculation of the enhancement factor.** The EF was calculated according to the formula:

$$EF = (I_{SERS}/N_{SERS})/(I_{bulk}/N_{bulk}) \quad (1)$$

$$N_{SERS} = CVN_A A_{Raman}/A_{sub} \quad (2)$$

$$N_{bulk} = \rho h A_{Raman} N_A/M \quad (3)$$

$N_{SERS}$ and $N_{bulk}$ denote the number of R6G molecules that contribute to the signal intensity, enhanced and normal, respectively, while $I_{SERS}$ and $I_{bulk}$ denote the corresponding enhanced and normal Raman intensities. For analyte molecules loaded with SERS-active substrates, $N_{SERS}$ can be estimated by equation 2, assuming that the analyte were distributed uniformly on the surface of substrates. $C$ is the molar concentration of the analyte solution, $V$ is the volume of the droplet, $N_A$ is Avogadro constant. $A_{Raman}$ is the laser spot area (1 μm in diameter) of Raman scanning. Twenty microliters of the droplet on the substrate was spread into a circle of about 3 mm in diameter after solvent evaporation, from which the effective area of the substrate, $A_{Sub}$, can be obtained. The data for bulk R6G crystals on bare $Si/SiO_2$ wafer were used as normal Raman reference. The confocal depth ($h$) of the laser beam into bulk crystal is 21 μm [1], and on the basis of molecular weight ($M$) and density ($\rho$) of bulk R6G (1.15 g $cm^{-3}$), the $N_{bulk}$ is calculated by equation 3.

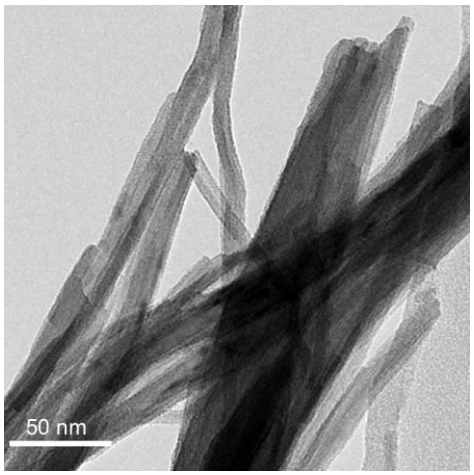


**Figure S1** TEM image of $W_{18}O_{49}$ nanowires.

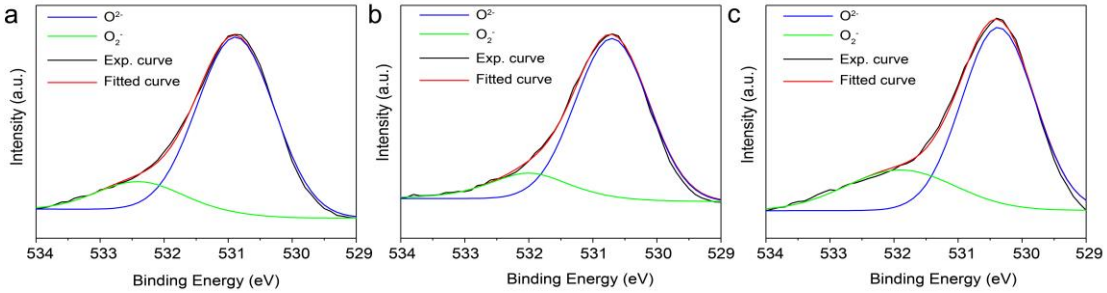


**Figure S2** XPS spectra of O 1s levels for (a) $W_{18}O_{49}$, (b) Ag-$W_{18}O_{49}$ and (c) Pt-$W_{18}O_{49}$ samples.

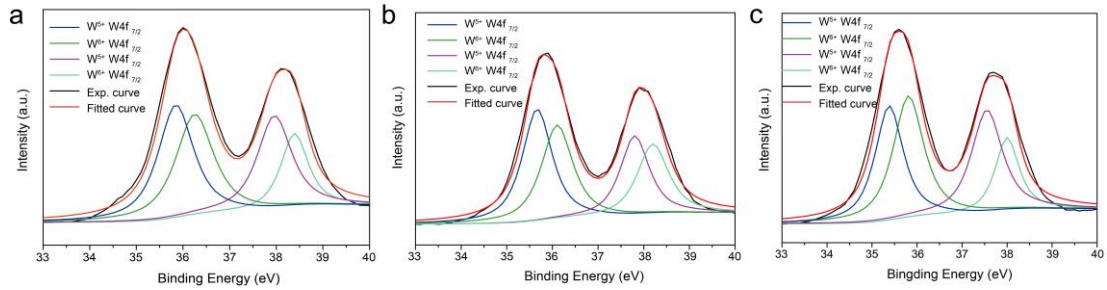


**Figure S3** XPS spectra of W4f core levels for (a) $W_{18}O_{49}$, (b) Ag-$W_{18}O_{49}$ and (c) Pt-$W_{18}O_{49}$ samples.

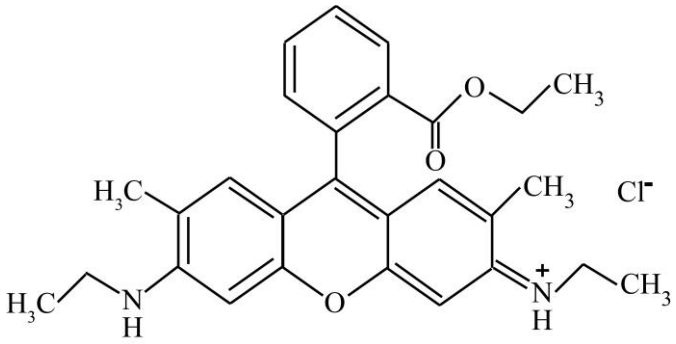


**Figure S4** Chemical structure of Rhodamine 6G (R6G).

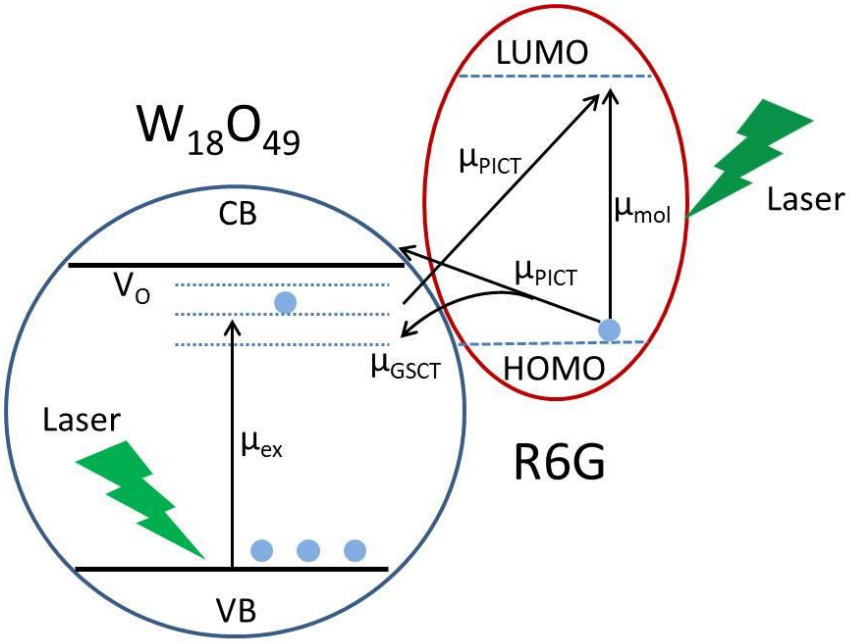


**Figure S5** Energy-level diagram of R6G on pristine $W_{18}O_{49}$ with respect to vacuum, demonstrating the SERS properties based on the charge-transfer transitions in relationship with oxygen vacancies and trapped states. Upon band-level alignment between $W_{18}O_{49}$ and R6G, contributions from several types of thermodynamically feasible charge-transfer resonances may be in relation with the SERS properties of the pristine $W_{18}O_{49}$ substrate upon excitation at 532 nm, including molecule resonance ($\mu_{mol}$) of R6G, exciton resonance ($\mu_{ex}$) of $W_{18}O_{49}$ defect states (Vo), and the photon induced charge transfer resonance ($\mu_{PICT}$) together with the ground-state charge transfer resonance ($\mu_{GSCT}$) from matched energy level between $W_{18}O_{49}$ and R6G molecules. These charge-transfer transitions would be brought in resonance with the incident laser, which leads to the enhancement of Raman-scattering cross section

of R6G molecule.

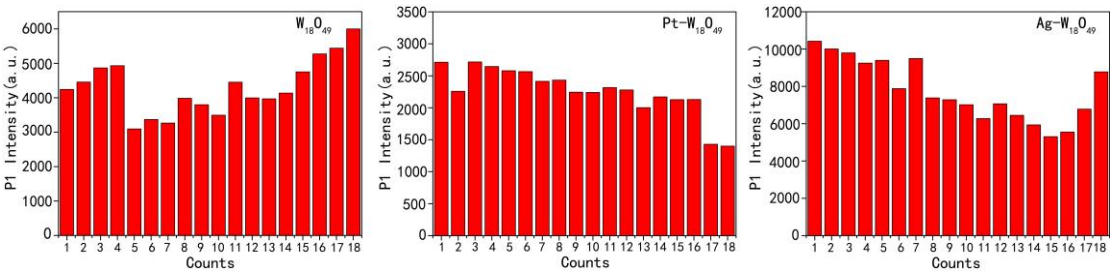


**Figure S6** The intensities of the P1 (612 $cm^{-1}$) Raman vibration mode of R6G on varied spots from $W_{18}O_{49}$, Ag-substrates and Pt-$W_{18}O_{49}$. SERS enhancement of each substrate was examined with data acquired by recording spectra at 18 stochastic spots at different locations across one substrate. EF value for each substrate was calculated from the average intensity of P1 peak.

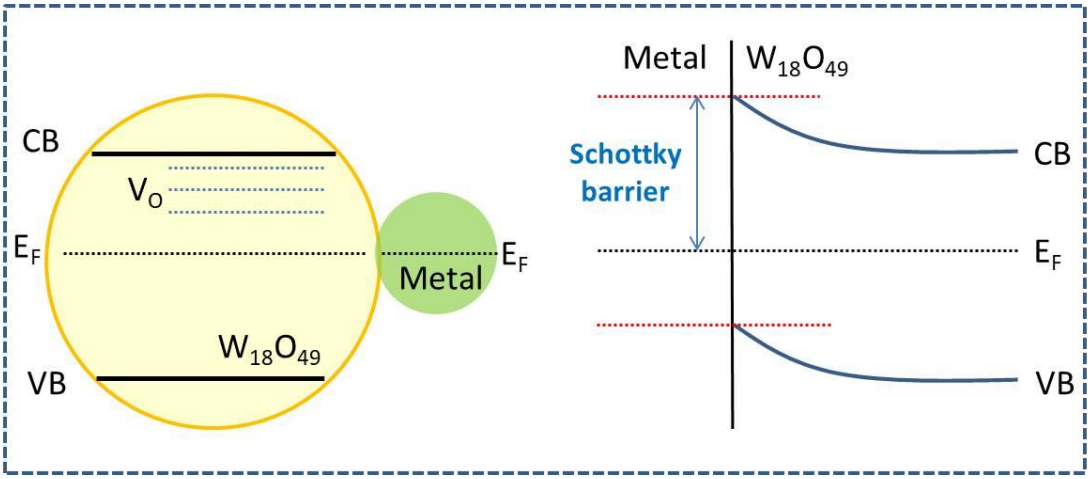


**Figure S7** Energy band diagrams of the metal-$W_{18}O_{49}$ junction with charge equilibration in the dark. When metal nanoparticles are in physical contact with $W_{18}O_{49}$, electrons are transferred between $W_{18}O_{49}$ and metal nanoparticles to equilibrate the Fermi levels. Especially, a large Schottky barrier can be expected at the Pt-$W_{18}O_{49}$ interface driven by the large difference in work functions between Pt and $W_{18}O_{49}$.

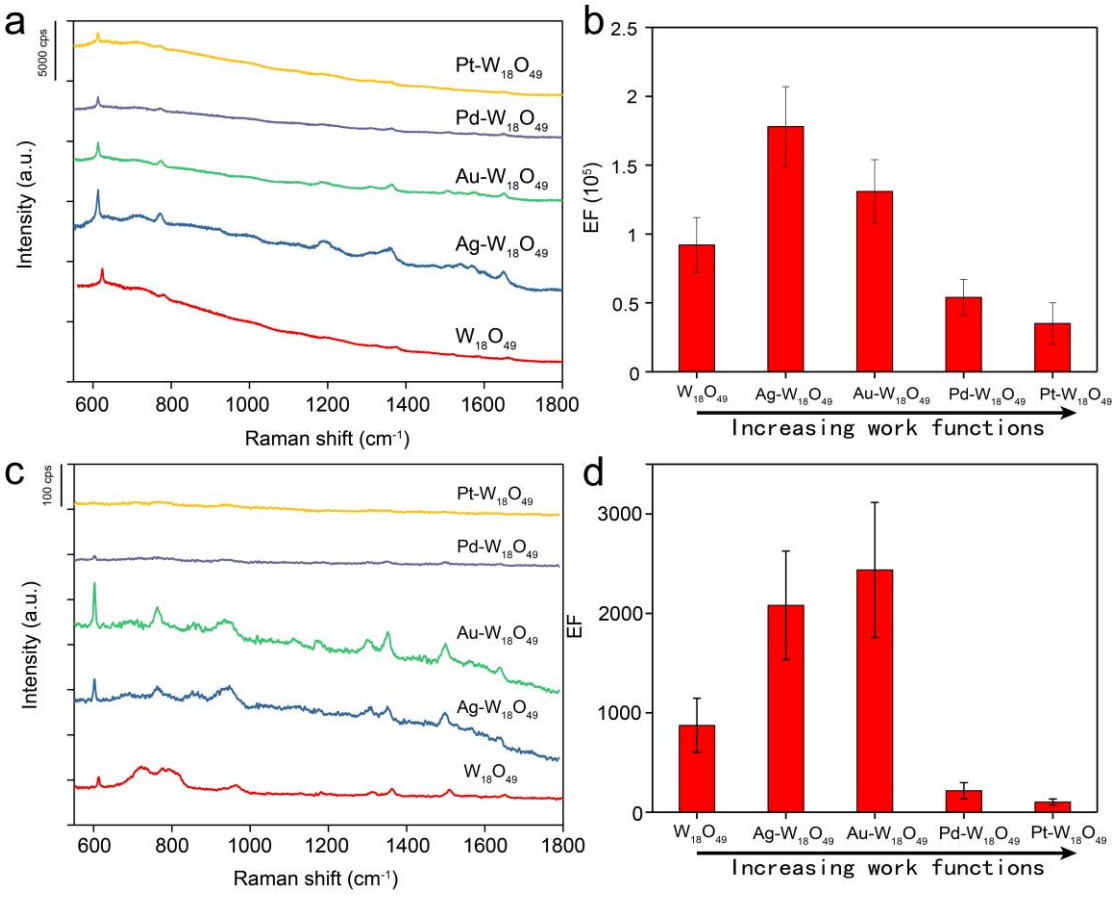


**Figure S8** (a) Raman spectra of R6G and (b) EFs for the vibration mode P1 (612 $cm^{-1}$) on $W_{18}O_{49}$ and metal-loaded $W_{18}O_{49}$ samples under 532 nm excitation. (c) Raman spectra of R6G and (d) EFs for the vibration mode P1 (612 $cm^{-1}$) on $W_{18}O_{49}$ and metal-loaded $W_{18}O_{49}$ samples under 633 nm excitation. The order of the substrates on the x-axes are arranged according to the order of the work functions of the metal components, Ag (4.26 eV) << Au (5.1 eV) ≤ Pd (5.12 eV) < Pt (5.65 eV).

To examine the excitation wavelength dependence, SERS signals of R6G ($10^{-5}$ M) with five substrate materials (pristine $W_{18}O_{49}$, Ag-$W_{18}O_{49}$, Au-$W_{18}O_{49}$, Pd-$W_{18}O_{49}$, Pt-$W_{18}O_{49}$) are examined and compared under excitation at 532 nm and 633 nm, respectively. The comparison results illustrate several points: (1) For all samples, SERS signals are greatly weakened under 633 nm excitation when compared with those obtained under 532 nm excitation. This wavelength-depended phenomenon may be largely ascribed to the off-resonance of possible allowed transitions, e.g. molecule transitions (530 nm) in R6G, for excitation at 633 nm. (2) Comparing to the pristine

$W_{18}O_{49}$ sample, the SERS enhancements of Ag-$W_{18}O_{49}$ and Au-$W_{18}O_{49}$ are further increased, while Pd-$W_{18}O_{49}$ and Pt-$W_{18}O_{49}$ show clearly a decrement in SERS enhancements, no matter what laser is used for the SERS measurements. The trends observed are in close relationship with the interfacial electron flows between $W_{18}O_{49}$ and metal components under laser irradiation. As demonstrated in the main text, Ag and Au nanoparticles exhibiting PRET effect upon visible light irradiation may help to populate the electrons at the surface of $W_{18}O_{49}$ in contact, leading to the observed SERS enhancement. In contrast, Pd and Pt nanoparticles with only weak LSPR absorption in the UV region have no PRET effect under visible light excitation, instead, Schottky barrier formed between $W_{18}O_{49}$ and metal nanoparticles with large work functions results in an obvious decrement in the electron population of $W_{18}O_{49}$, and thus the significantly decreased SERS signals. As a matter of fact, it is the visible light excitation in SERS measurements that causes different electron flows between Ag, Au and Pd, Pt when in contact with $W_{18}O_{49}$, so this charge-transfer process in our metal-$W_{18}O_{49}$ system is believed to be wavelength dependent. (3) Another noticeable point is that the EF value of Au-$W_{18}O_{49}$ is slightly larger than that of Ag-$W_{18}O_{49}$ using 633 nm excitation, while the reversed trend is found using 532 nm excitation. Such a change with different excitation wavelengths may be largely ascribed to the interfacial charge-transfer induced by PRET effects from Au and Ag metals, which are in resonance with different excitation wavelengths. Also, it should be mentioned that EM contribution from noble metals has already been excluded in our composites due to the relative small loading amount of metals, as already demonstrated in the main text.

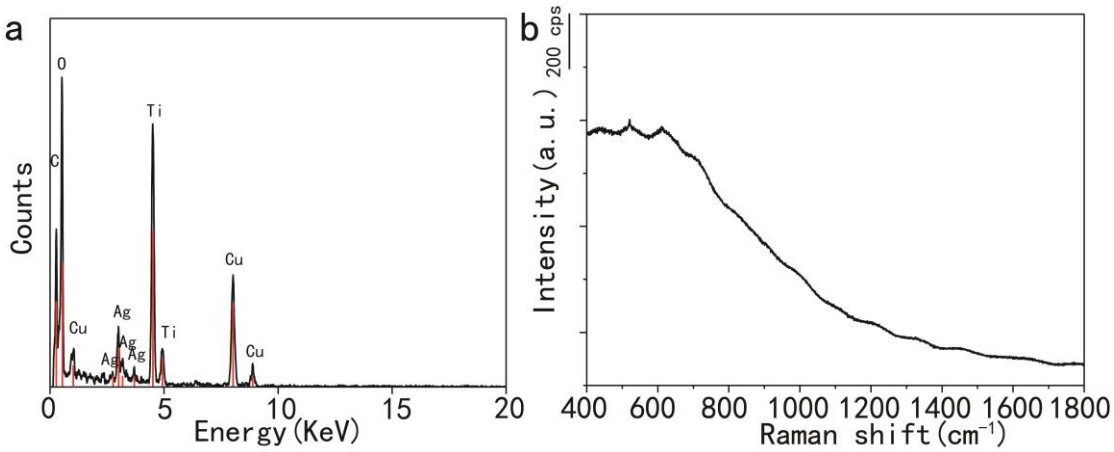


**Figure S9** EDX spectrum of Ag-$TiO_2$ sample, showing the loading of Ag particles on $TiO_2$. Ag-$TiO_2$ sample shows negligible Raman signals for the detection of $10^{-5}$ M R6G.

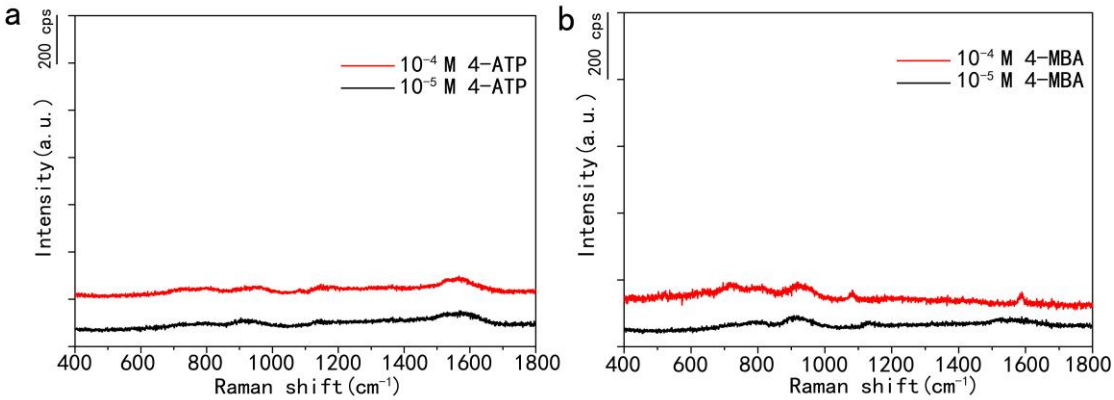


**Figure S10** SERS signals for the detection of (a) 4-ATP and (b) 4-MBA on the Ag-$W_{18}O_{49}$ substrate, at the concentration of $10^{-5}$ and $10^{-4}$ M, respectively.

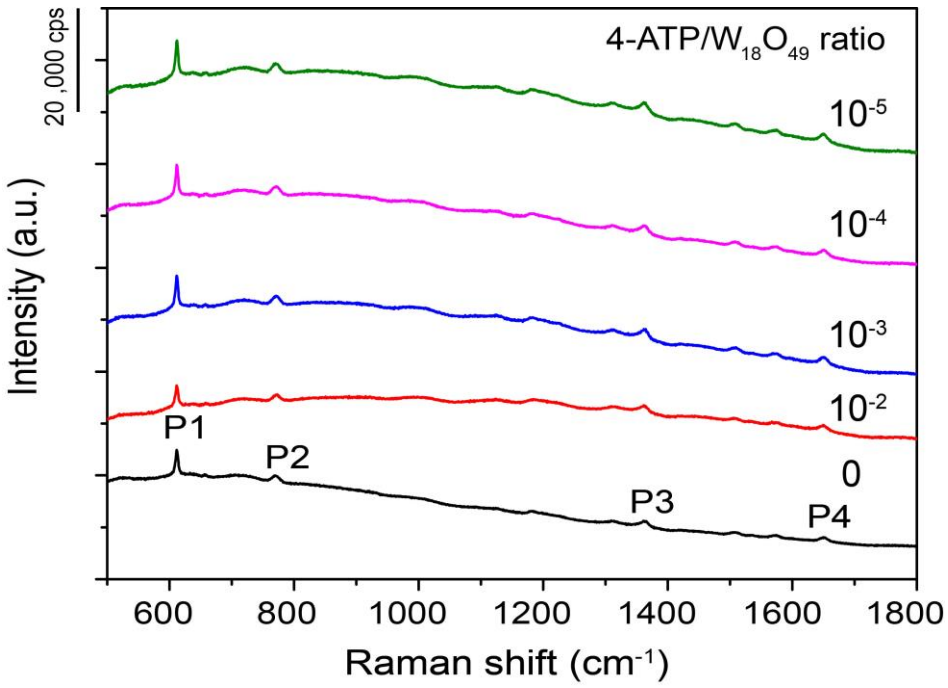


**Figure S11** Raman signals of $10^{-5}$ M R6G for pristine $W_{18}O_{49}$ and that pre-combined with 4-ATP at a 4-ATP/$W_{18}O_{49}$ ratio ranging from $10^{-5}$ to $10^{-2}$.

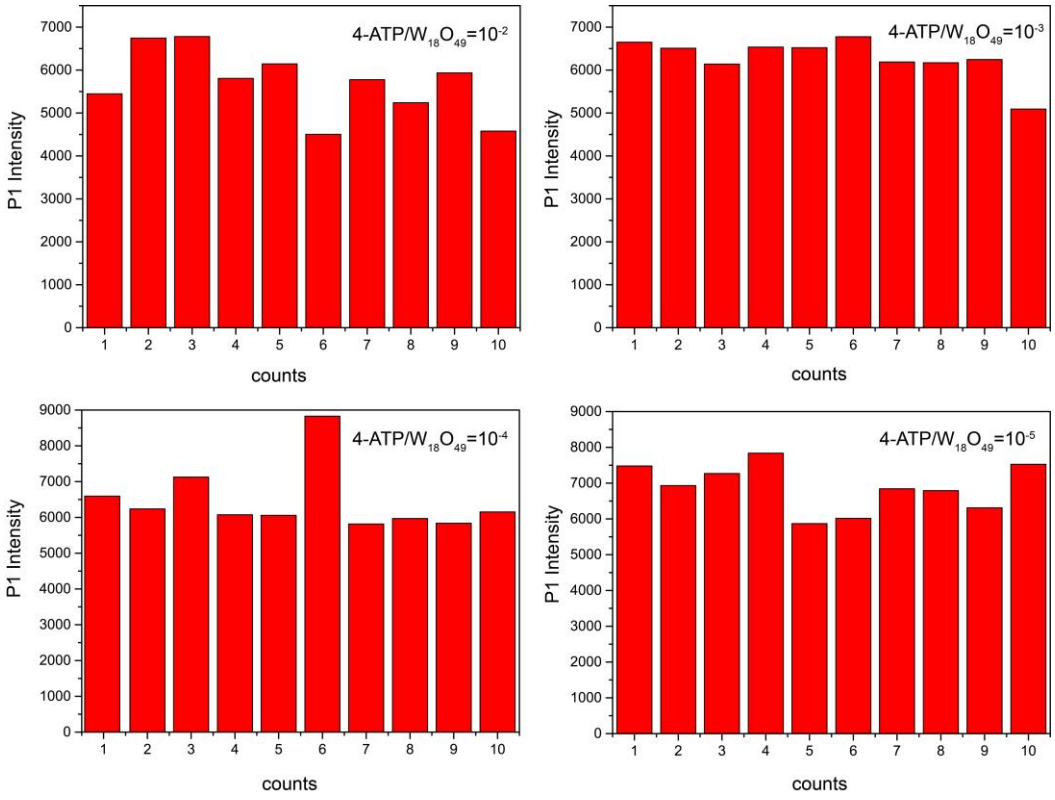


**Figure S12** The intensities of the P1 (612 $cm^{-1}$) Raman vibration mode of R6G on varied spots from 4-ATP modified $W_{18}O_{49}$ substrates. Substrates with a 4-ATP/$W_{18}O_{49}$ ratio (wt%) ranging from $10^{-5}$ to $10^{-2}$ were examined with data

acquired by recording spectra at 10 stochastic spots at different locations across one substrate. EF value for each substrate was calculated from the average intensity of P1 peak.

**Table S1** Atomic ratio for tungsten in different valence states, and the Ag/W or Pt/W ratio of the samples obtained by XPS and ICP-MS measurements.

| Sample | Atomic ratio of $W^{5+}/W^{6+}$ | Relative loading amounts of Ag/Pt towards $W_{18}O_{49}$ (wt%) |
|---|---|---|
| $W_{18}O_{49}$ | 0.81 | ---- |
| Ag-$W_{18}O_{49}$ | 0.91 | 1.1 |
| Pt-$W_{18}O_{49}$ | 0.85 | 0.9 |

**Supplementary References**


[1] S. Cong, Y. Y. Yuan, Z. G. Chen, J. Y. Hou, M. Yang, Y. L. Su, Y. Y. Zhang, L. Li, Q. W. Li, F. X. Geng, Z. G. Zhao, *Nat. Commun.*, 2015, **6**, 7800.

[2] A. Fujii, Z. C. Meng, C. Yogi, T. Hashishin, T. Sanada, K. Kojima, *Surf. Coat. Tech.*, 2015, **271**, 251-258.